An Energy-Based Localization Theory

Part II – Effects of the Diffusion, Inertia and Dissipation Numbers

By

H.P. Cherukuri and T.G. Shawki

Department of Theoretical and Applied Mechanics
University of Illinois at Urbana–Champaign
Urbana, Illinois 61801

ABSTRACT

The basic framework for an energy–based theory of localization in dynamic viscoplasticity was recently developed by Cherukuri and Shawki (1993). In this framework, the total kinetic energy serves as a single parameter for the characterization of the full localization history. A characteristic evolution profile of the kinetic energy was shown to correspond to a localizing deformation. Here, we implement the foregoing characterization of localization towards the improved understanding of the mechanics of shear band formation. In particular, we examine the influence of three primary dimensionless groups on localization. These groups are referred to as the inertia number, the diffusion number and the dissipation number. The limits of applicability of the quasi–static assumption as well as the adiabatic deformation assumption are also addressed. Computational evidence indicate that the dissipation number plays a significant role in determining the material localization sensitivity.

1. Introduction

The failure of engineering materials during modern severe operating conditions has been a focal point for engineering research in the past decade. Among the phenomena that are intimately connected to catastrophic structural failure is the localization of plastic flow into narrow spatial bands (known as the *shear bands*). This observation explains the current interest in resolving various questions related to the onset and late−time behavior of shear localization in dynamic deformations. Shawki and Clifton (1989) presented a review of the different mechanisms believed to explain shear band formation in a wide spectrum of materials and loading rates. Shawki (1992) presented a review of the various characterizations of shear localization in dynamic viscoplasticity.

An energy−based framework for the analysis of shear localization in dynamic viscoplasticity was recently developed by Shawki (1993a,b) for the pre−localization regime and later extended by Cherukuri and Shawki (1993) to encompass the complete localization history. This framework uses the system total kinetic energy as a single parameter that is capable of characterizing the full localization process. Table 1 presents a chronological summary of the development of the energy−based localization theory. Shawki (1993a) illustrated, through a time−dependent linear perturbation analysis, that a positive rate of change of the kinetic energy of absolute perturbations is a necessary and sufficient condition for the linear solution − including the effects of spatial perturbations − to deviate from the underlying homogeneous solution. This result represented the early indication to the possible role of kinetic energy towards the characterization of localization. In fact, in a subsequent article, Shawki (1993b) used the energy−based onset criterion to reproduce a large number of necessary localization conditions that were earlier derived by other authors using drastically different viewpoints of localization. The success of this approach within the linear stability context motivated further pilot numerical studies by Zbib and Jubran (1992) and by Shawki, et al (1992). These pilot

studies confirmed expectations that the system kinetic energy plays a significant role as far as characterizing the complete localization history.

Table 1 – A chronological summary of developments in the energy–based localization theory.

Development	Methodology	Authors	Year
Recognition of the positive kinetic energy rate as a necessary condition for the onset of localization.	*Time–dependent, linear stability analysis*	T.G. Shawki	1988 (1993a)
Derivation of analytic initiation conditions for large classes of materials based on the energy criterion.	*Time–dependent, linear stability analysis*	T.G. Shawki	1988 (1993b)
Early numerical observations of the connection between final failure and the evolution of the system kinetic energy.	*Three–dimensional, nonlinear finite element solutions.*	H.M. Zbib J.S. Jubran	1992
A Review of the various characterizations of shear localization in dynamic viscoplasticity.	*Linear and nonlinear analysis.*	T.G. Shawki	1992
Early Numerical Results confirming the role of the kinetic energy throughout the entire localization history.	*One–dimensional, nonlinear finite difference solutions.*	T.G. Shawki R.A. Sherif H.P. Cherukuri	1992
A formal analysis of the energy–based theory of localization including details of the used numerical algorithm.	*One–dimensional, nonlinear analysis and finite difference solutions.*	H.P. Cherukuri T.G. Shawki	1993
Implementation of the energy–based theory towards a consistent parametric study of the effects of the inertia, diffusion and dissipation dimensionless numbers on localization.	*One–dimensional, nonlinear finite difference solutions of the governing equations for simple shearing motion.*	H.P. Cherukuri T.G. Shawki	present article

Cherukuri and Shawki (1993), in part I of this work, have presented the formal energy–based framework along with example calculations through which a number of *critical times* were defined. In the foregoing work, three dimensionless groups were identified and termed the inertia number, the diffusion number and the dissipation number. Further details regarding these groups are provided in the next section. Furthermore, Cherukuri and Shawki (1993) presented the details of a finite difference scheme used for the numerical integration of the system of nonlinear equations governing the dynamic, one–dimensional simple shear of a thermally–sensitive, viscoplastic material. A convergence analysis of the finite difference

algorithm was presented along with a discussion that illustrates the implementation of the energy–based characterization of localization towards finding sufficient convergence conditions. An example calculation was presented to aid the definitions of various critical strains along the localization history.

In this paper, we take advantage of the aforementioned developments and conduct a consistent parametric study of the effects of the three dimensionless groups (the inertia, diffusion and dissipation numbers) on localization. Moreover, we present a numerical examination of the effect of the applied strain rate on localization. Here, we note that the numerical method used throughout this work is that described by Cherukuri and Shawki (1993).

2. The Model

Figure (1) illustrates an inifinite homogeneous plate of thickness H in the $\hat{x}$ −direction while it extends indefinitely in the other two cartesian coordinate directions. The upper face of the plate is subjected to a constant velocity while the lower face is fixed. The system of governing equations is given by (see Shawki and Clifton (1989) for further details)

$$\hat{\varrho}_0 \frac{\partial \hat{v}}{\partial \hat{t}} = \frac{\partial \hat{\sigma}}{\partial \hat{x}} \tag{1}$$

$$\frac{\partial \hat{\sigma}}{\partial \hat{t}} = \hat{\mu}\left\{\frac{\partial \hat{v}}{\partial \hat{x}} - \hat{\dot{\gamma}}^{P}\right\} \tag{2}$$

$$\frac{\partial \hat{\theta}}{\partial \hat{t}} = \hat{r}_0 \frac{\partial^2 \hat{\theta}}{\partial \hat{x}^2} + \hat{r}_1 \hat{\sigma} \hat{\dot{\gamma}}^{P}, \tag{3}$$

$$\hat{\dot{\gamma}}^{P} = \hat{\phi}\ (\hat{\sigma}, \hat{\gamma}, \hat{\theta}) \qquad \text{or} \qquad \hat{\sigma} = \hat{\psi}\ (\hat{\dot{\gamma}}^{P}, \hat{\gamma}, \hat{\theta}) \tag{4}$$

where

$$\hat{r}_0 = \frac{\hat{K}}{\hat{\varrho}_0 \hat{c}}, \qquad \hat{r}_1 = \frac{\beta}{\hat{\varrho}_0 \hat{c}} \tag{5}$$

Equation (1) expresses the balance of linear momentum, equation (2) is the kinematic compatibility equation, equation (3) represents the energy balance and, equation (4) provides alternative representations of the material thermal viscoplastic response.Furthermore, $\hat{v}$ is the particle velocity in the $\hat{x}$ direction, $\hat{\sigma}$ is the shear stress $\hat{\sigma}_{\hat{x}\hat{y}}$, $\hat{\theta}$ is the absolute temperature, $\hat{\gamma}^{P}$ is the plastic strain, $\hat{\mu}$ is the elastic shear modulus, $\hat{\varrho}_0$ is a constant material density, $\hat{K}$ is a constant heat conduction coefficient, $\hat{c}$ is the specific heat and β is a non−negative scalar, whose value is less than unity, which expresses the amount of plastic dissipation that is converted to heat.

It is convenient to express equations (1) through (4) in a dimensionless form. Non−dimensionalisation is conducted so that the form of the governing equations remains unchanged.

The dimensionless quantities are defined by

$$t = \frac{\hat{t}}{\hat{t}_0}, \quad x = \frac{\hat{x}}{H}, \quad \sigma = \frac{\hat{\sigma}}{\hat{\sigma}_0}, \quad v = \frac{\hat{v}\hat{t}_0}{H}, \quad \dot{\gamma}^p = \frac{\hat{\dot{\gamma}}^p}{\hat{\dot{\gamma}}_0^p}, \quad \theta = \frac{\hat{\theta}}{\hat{\theta}_0},$$

$$K = \frac{\hat{K}\hat{\theta}_0\hat{t}_0}{\hat{\sigma}_0 H^2}, \quad \varrho_0 = \frac{\hat{\varrho}_0 H^2}{\hat{\sigma}_0 \hat{t}_0^2}, \quad c = \frac{\hat{c}\hat{\theta}_0\hat{t}_0^2}{H^2}, \quad \mu = \frac{\hat{\mu}}{\hat{\sigma}_0}, \quad r_0 = \frac{\hat{k}\hat{t}_0}{\hat{\varrho}\hat{c}H^2}, \quad r_1 = \frac{\beta\hat{\sigma}_0}{\hat{\varrho}\hat{c}\hat{\theta}_0}. \tag{6}$$

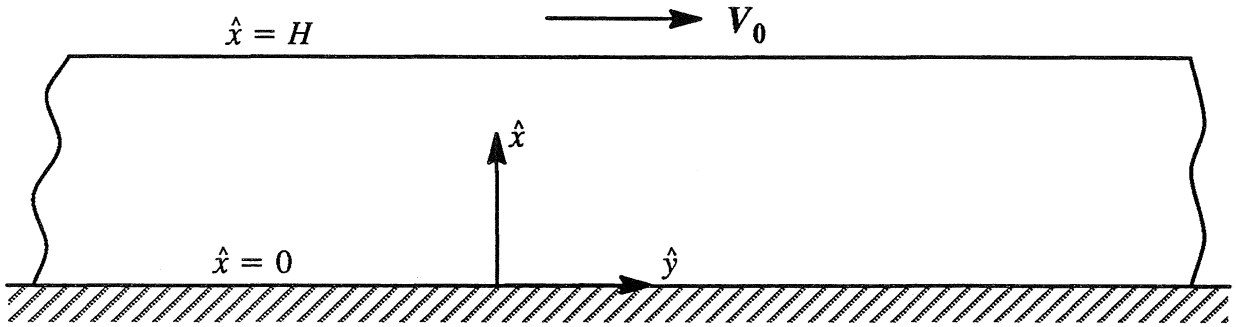

Figure (1) – A schematic illustration of a one–dimensional simple shearing motion

In equation (6), quantities with the subscript "0" denote appropriately–selected reference values (e.g. values that the dimensional field variables have in a homogeneous deformation at the time that a perturbation is introduced). The characteristic time $\hat{t}_0$ is the time required to obtain a unit shear strain at the strain rate $\hat{\dot{\gamma}}_0^p$. The foregoing dimensionless quantities will be used in the remainder of this work. Field variables will appear without the superposed "hat" which implies usage of dimensionless quantities throughout the discussion.

At this point, it is useful to note that the dimensionless groups ϱ_0, r_0 and r_1 are analogous to the dimensionaless numbers commonly encountered in fluid mechanics, namely, the Reynolds number, inverse of the Peclet number and the ratio of Eckert number and Reynolds number respectively. In the current context, we rename the foregoing quantities to the *inertia number* for ϱ_0, *diffusion number* for r_0, and *dissipation number* for r_1. Next, an attempt is made to emphasize the relevant physical interpretation of these various numbers.

2.1. Physical interpretation of the dimensionless numbers

Since ϕ_0 is the inverse of t_0, the inertia number ϱ_0 can be rewritten as the ratio of inertial effects to viscous effects; that is

$$\varrho_0 = \frac{(\hat{\varrho}_0 \hat{V}_0 H)}{(\hat{\sigma}_0/\hat{\phi}_0)} = \frac{\text{inertial effects}}{\text{viscous effects}}. \tag{7}$$

Thus, larger values of the applied strain rate correspond to larger inertia numbers. In the following sections, we will illustrate that larger inertia numbers result in a delay in localization initiation as long as the other dimensionaless numbers remain constant. Small inertia numbers correspond to deformations in which viscous effects dominate inertial effects which is analogous to the creeping flow of fluid mechanics. In this case, inertial effects can be ignored in the analyses predicting the onset of severe localization. The Kolsky bar tests – in general – fall in the domain of very small inertia numbers. Thus, for these tests, the quasi–static assumption appears to be a reasonable approximation for both analytical and/or numerical investigations of the onset of severe localization.

The diffusion number is the inverse of Peclet number (which is the product of the Reynolds and Prandtl numbers). Thus, it can be rewritten as

$$r_0 = \frac{\hat{\sigma}_0}{\hat{\varrho}_0 \hat{V}_0^2} \cdot \frac{\hat{k}/\hat{c}}{(\hat{\sigma}_0/\hat{\phi}_0)} \tag{8}$$

We note that the Prandtl number is the ratio of some measures of viscous and diffusion effects. The larger (smaller) the Prandtl (diffusion) number, the weaker is the diffusion effect. Weak diffusion effect implies that the amount of thermal energy flowing across a unit distance with an overall temperature difference of 1 K is much smaller than the energy required to raise a unit specimen's length by 1 K. Thus, smaller diffusion numbers are associated with a higher tendency towards adiabatic behavior. However, we shall illustrate that, regardless of how large

this number is, the adiabatic deformation assumption breaks down once severe localization takes place.

The dissipation number can be expressed in the form

$$r_1 = \frac{\beta\hat{\sigma}_0}{\hat{\varrho}\hat{c}\hat{\theta}_0} = \frac{\beta\hat{\sigma}_0\hat{\phi}_0\hat{t}_0}{\hat{\varrho}\hat{c}\hat{\theta}_0} \tag{9}$$

Thus, the dissipation number is the ratio of the thermal energy produced in time $\hat{t}_0$ per unit volume over the energy required to raise the temperature of a unit volume by $\hat{\theta}_0$. Hence, for two different solids subjected to the same applied strain rate at the same test temperature, since the heat capacity is the same, the material with the higher yield stress has a higher dissipation number. For example, the hot−rolled steel HRS−1020 has a yield stress that is 3 times less than that of HY−100 steel. In this case, the dissipation number for HY−100 steel is 3 times larger than that of the HRS steel. Athough the energy required to raise the temperature by a finite amount is the same for both steels, the dissipation in HY−100 steel is more than that in HRS steel indicating that localization might occur faster in the former than in the latter. This observation will be confirmed through our numerical results in the future sections. Here, we note that a similar observation has been reported by Marchand and Duffy (1988).

2.2. Boundary and Initial Conditions

The considered boundary conditions consist of thermally−insulated and velocity−controlled boundaries. This is expressed mathematically as follows:

$$v(0,\ t) = 0, \quad v(1,\ t) = 1, \quad 0 \le t < \infty, \tag{10}$$

$$\theta_{,x}(0,\ t) = \theta_{,x}(1,\ t) = 0, \quad 0 \le t < \infty. \tag{11}$$

The assumption of insulated boundaries is expected to closely simulate the thermal state associated with the Kolsky bar–type tests. A consequence of the insulated boundary conditions is that the posed boundary–value problem has a spatially–homogeneous solution as opposed to the case of isothermal boundary conditions for which a homogeneous solution does not exist.

The initial conditions are chosen to correspond to a slightly perturbed homogeneous state. The perturbation is assumed to model geometric and/or material inhomogeneities. The set of considered initial conditions is given by

$$v(x,0) = x, \tag{12}$$

$$\dot{\gamma}^{p}(x,0) = 1, \tag{13}$$

$$\gamma(x,0) = \gamma_0, \tag{14}$$

$$\theta(x,0) = 1 + \varepsilon f(x), \tag{15}$$

$$\sigma(x,0) = \psi\ (1,\ \gamma_0\ ,1 + \varepsilon f(x)\ ), \tag{16}$$

for $0 \leq x \leq 1$. In equation (15), $f(x)$ is of order unity and represents the perturbation shape which is selected to be consistent with the boundary condition (11). Furthermore, a vanishing ε corresponds to an initial homogeneous state.

3. Diffusion Number and Localization

This section examines the effect of the diffusion number on the evolution of localization. First, we review the localization criteria derived by Shawki (1993b) using the linear perturbation analysis while accounting for the time−dependence of the homogeneous solution.

3.1. Localization criteria from linear perturbation analysis

We consider a power−law material given by

$$\sigma = (\theta)^{\nu} \left(\frac{\gamma}{\gamma_0}\right)^{n} (\dot{\gamma}^{p})^{m}, \tag{17}$$

For a strain−independent power law material ($n = 0$), the necessary condition for localization using linear perturbation analysis is shown to be (see Shawki (1993b))

$$r_1\left(\frac{\nu + m}{m}\right) + r_0\xi_n^2(1 + r_1(1 - \nu)t) < 0, \qquad \text{with} \qquad \nu < 1, \tag{18}$$

where $t \leq T$, while T denotes the maximum time before which the linear solution represents an acceptable approximation to the nonlinear solution and $\xi_n = n\pi$, $(n = 1, 2, 3, ...)$. The foregoing inequality indicates that, in the absence of heat conduction ($r_o = 0$), the necessary localization condition reduces to

$$\nu + m < 0. \tag{19}$$

Comparison of the inequalities (18) and (19) illustrates the stabilizing effect of the diffusion number as far as the onset of localization is concerned. Furthermore, for a given net softening effect (i.e. a given negative value of $\nu + m$), there exists a critical wavelength below which the initial disturbances will decay and no localization is anticipated. Now we note that if the diffusion number r_0 is sufficiently large, the necessary condition for localization (18) reduces to

$$1 + r_1(1 - \nu)t < 0, \ \nu < 1, \tag{20}$$

which is never realized, implying no tendency for localization. This conclusion can be extended to the case where $n \neq 0$ since sufficiently large diffusion implies a nearly constant temperature as evidenced by examining the energy balance equation (4). In such case, the power–law constitutive equation (17) reduces to

$$\sigma = (\frac{\gamma}{\gamma_0})^n \ (\dot{\gamma}^p)^m, \tag{21}$$

for which the necessary condition for localization obtained by Shawki (1993b) is

$$n + m < 0 \tag{22}$$

For strain–rate hardening solids, localization is possible for materials which exhibit strain softening such that the condition (22) is met. Computational experiments involving isothermal deformations of strain softening solids indicate that the strain rate may blow up in finite time leading to zero width band. This issue will be further discussed in later sections.

It is useful to note that "sufficiently large" diffusion numbers correspond to deformations in which diffusion effects are much stronger than viscous effects (while the inertia number is kept fixed). The numerical results shown in the following sections as well as the linear stability results by Shawki (1993b) indicate that the diffusion number plays a major role in determining the shear band thickness. This observation has been first noted by Merzer (1982) through his numerical solutions of the fully nonlinear system.

3.2. Shear band width and the diffusion number

This section discusses the role of the diffusion number towards setting a length scale for the evolving localized zones. It is important to note that, during high rates of loading of visco-plastic materials, the band "width" evolves continuously. Moreover, there is no clear boundary that separates the localizing zone from the remainder of the body. Hence, the evolution of smooth localizing solutions gives rise to a degree of uncertainty as far as the shear band width is

concerned. As a result, a variety of definitions for the band width have been proposed. Wright (1987) defines the shear band width as the width of the region from the position of maximum strain rate (in the localized zone) to the point, on either side of this position, at which the strain rate drops by 10 percent. Sherif and Shawki (1992), Wright (1992), Dodd and Bai (1985) considered steady state solutions of the simple shearing motion and obtained approximate expressions for the band width. Gioia and Ortiz (1992) considered the steady state behavior of a two–dimensional half–space problem subjected to constant velocity at the boundary. They defined the band width as the width of the region near the surface bounded by the free surface and the surface at which the velocity is 0.99 times the boundary velocity.

In the context of the energy–based theory, Cherukuri and Shawki (1993) – part I of this paper – have presented a number of critical times during the late stages of evolution. Of particular interest is the so–called *stabilization time*, t_{stb}, at which the plastic strain rate attains its maximum value within the localizing zone. Cherukuri and Shawki (1993) have noted that the width of the evolving band decreases monotonically until t_{stb} is reached. For times greater than t_{tsb} the shear band width increases. We select the shear band width to correspond to the value it attains at the time $t = t_{stb}$. Further details on this selection can be found in part I of this work by Cherukuri and Shawki (1993).

At this point, we attempt to rationalize the observed, late–time strain rate drop for times greater than t_{tsb}. For this purpose, we derive the time rate of change of the flow stress, using the constitutive equation (4)–b, to obtain the identity

$$\frac{\partial \sigma}{\partial t} = S_1 \frac{\partial \dot{\gamma}^p}{\partial t} + S_2 \frac{\partial \theta}{\partial t} + S_3 \frac{\partial \gamma^p}{\partial t}, \tag{23}$$

where

$$S_1 \equiv \frac{\partial \sigma}{\partial \dot{\gamma}^p}, \quad S_2 \equiv \frac{\partial \sigma}{\partial \theta}, \quad S_3 \equiv \frac{\partial \sigma}{\partial \gamma^p}. \tag{24}$$

Taking advantage of equations (2) and (3), equation (23) takes the instructive form

$$S_1 \frac{\partial \dot{\gamma}^p}{\partial t} = \mu \frac{\partial v}{\partial x} - (\mu + C_p)\dot{\gamma}^p - r_o S_2 \frac{\partial^2 \theta}{\partial x^2}, \tag{25}$$

where

$$C_p \equiv S_3 + r_1 \sigma S_2, \tag{26}$$

denotes the slope of the adiabatic stress−strain curve at constant strain rate. Expression (25) indicates that the increase or decrease of the plastic strain rate, for a strain−rate hardening material, depends on whether the right side of (25) is positive or negative. For structural engineering materials, during the pre−localization regime, the term $\mu + C_p$ remains positive (even when C_p is negative). Furthermore, the velocity gradient within the localizing zone remains positive while the diffusion number is positive. For thermally−softening materials, the term S_2 is always negative. Moreover, within the localizing zone, the second temperature gradient is negative. Therefore; the right side of expression (25) consists of two positive terms that are being offset by the third negative term. Examination of expression (25), in view of the foregoing remarks, implies that sufficiently large diffusion may have the capacity to retard the continued growth of the shear band strain rate. It is also evident that the "strength" of the diffusion term increases as the band width decreases. Hence, we anticipate that there exists a critical minimum band width at which the diffusion term in (25) balances the first two terms leading to a maximum value of the plastic strain rate. The attainment of such a maximum strain rate was illustrated by Cherukuri and Shawki (1993) through late−time numerical solutions of the fully nonlinear system of equations (1) through (4). The time at which diffusion effects begin to retard further localization was referred to as the stabilization time t_{tsb}. Finally, we note that at $t = t_{tsb}$, the strain rate attains the local maximum value (at the band center) given by

$$\dot{\gamma}^p_{\max} = \frac{\mu \frac{\partial v}{\partial x} - r_o S_2 \frac{\partial^2 \theta}{\partial x^2}}{C_p + \mu}. \tag{27}$$

Figure (2) shows the spatial distribution of $\partial^2\theta/\partial x^2$ for two different, late times while considering two different values of the diffusion number r_0. Figure (2) −(a) corresponds to the case

study presented by Cherukuri and Shawki (1993). Figure (2) −(b) corresponds to the same case except that the diffusion number is higher by an order of magnitude while all the other dimensionless numbers are kept constant. The plotting time t_1 is smaller than the critical time t_{cr} (at which the kinetic energy evolution profile passes through an inflection point). In fact, t_1 is less than t_{stb}. It is evident that the *smaller* the diffusion number, the *larger* is the heat flux gradient at the center of the band. Therefore; it seems reasonable to conclude that heat conduction effects assume a rather significant role during the later stages of localization. Such effects must be included in the model even if the diffusion number is numerically small.

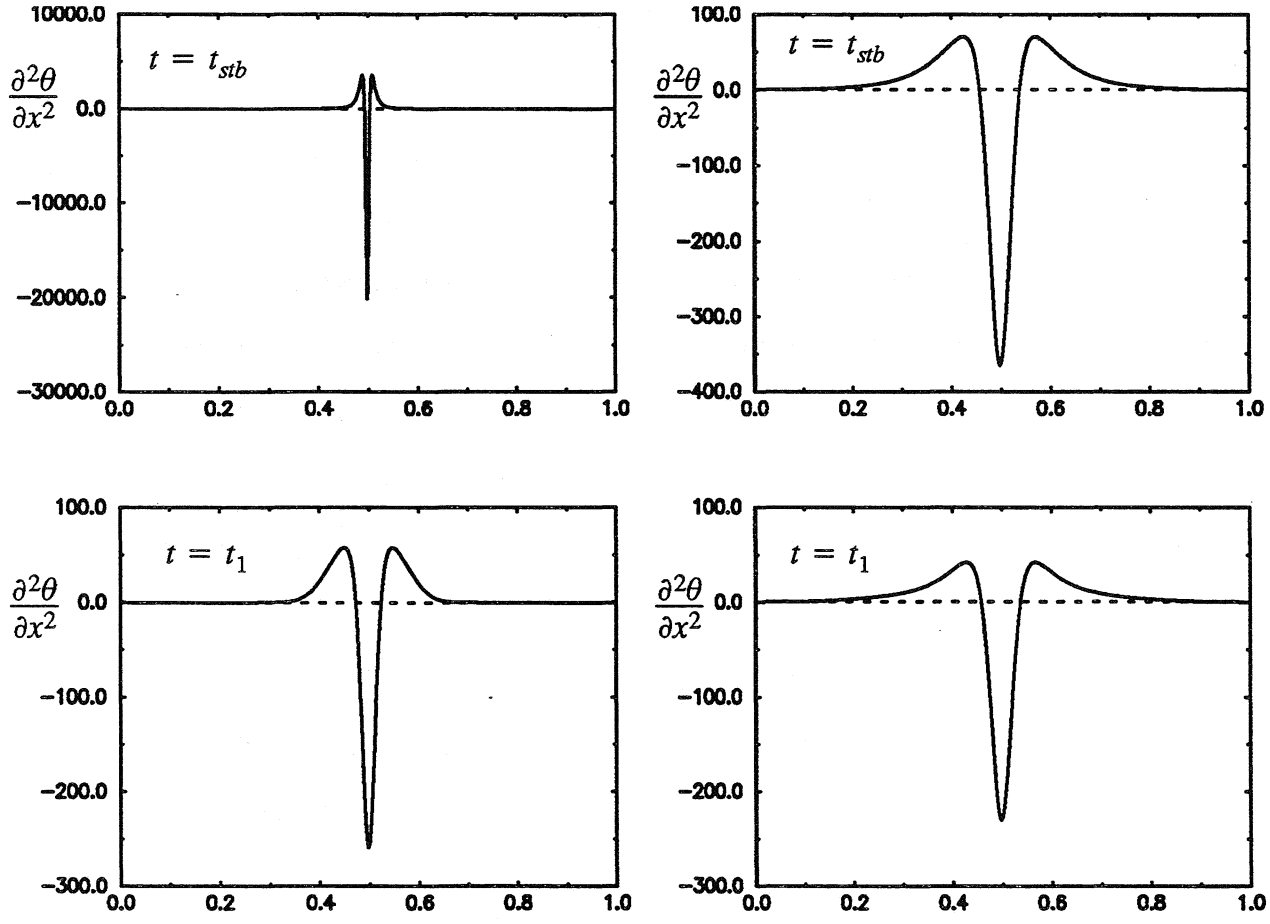

(*a*) $r_0 = 1.38 \times 10^{-3}$ (CRS steel)
$t_1 = 0.5$ and $t_{stb} = 0.6$

(*b*) $r_0 = 1.0 \times 10^{-2}$
$t_1 = 1.1$ and $t_{stb} = 1.30$

Figure (2) − A comparison of the effect of the diffusion number on the heat flux for two different late times.

For small values of the diffusion number (much less than unity), heat conduction effects are relatively weak during the pre–localization regime and can; therefore, be ignored. However, if post–localization modeling is required, those effects should be accounted for. The judgement regarding the relative effect of heat conduction requires a thorough knowledge of the localization phenomenon and must not be done arbitrarily.

It is interesting to observe that within the core of the localized zone (below the dashed lines), the temperature rise is caused by plastic dissipation (since $\partial^2\theta/\partial x^2$ is negative) whereas outside the core the temperature rise is caused by heat conduction (since $\partial^2\theta/\partial x^2$ is positive). Finally, it is useful to note that the diffusion number introduces a *thermal length scale* which is given by

$$\Lambda_{thermal} = \frac{\hat{\Lambda}_{thermal}}{H} = \sqrt{r_0} \tag{28}$$

Thus, if the shear band width is set by the above thermal length scale (whatever the definition of the band width may be) then the band width must be proportional to $\Lambda_{thermal}$; i.e.,

$$w = \Lambda_{thermal}\, f(...) \tag{29}$$

where $f(...)$ is a dimensionless function which depends on the inertia number, the dissipation number, the shear modulus and the loading conditions at the stabilization time t_{stb}. It should be noted that expression (29) is postulated in view of our numerical observations besides being supported by the results of the steady–state shear band model derived by Sherif and Shawki (1992).

3.3. Localization and the diffusion number

The effect of the diffusion number on localization is explored through several numerical experiments corresponding to different values of r_0 while keeping ϱ_0 and r_1 fixed. The data for the cold rolled steel remains the same as those used by Cherukuri and Shawki (1993) except for

changing r_0. In Figure (3) , the stress at the center of the band is plotted against the nominal strain for various values of r_0. In all the cases, $\dot{K}(t)$ reaches a maximum just when the stress begins to drop sharply, again confirming its validity as a single scalar quantity for characterizing severe localization.

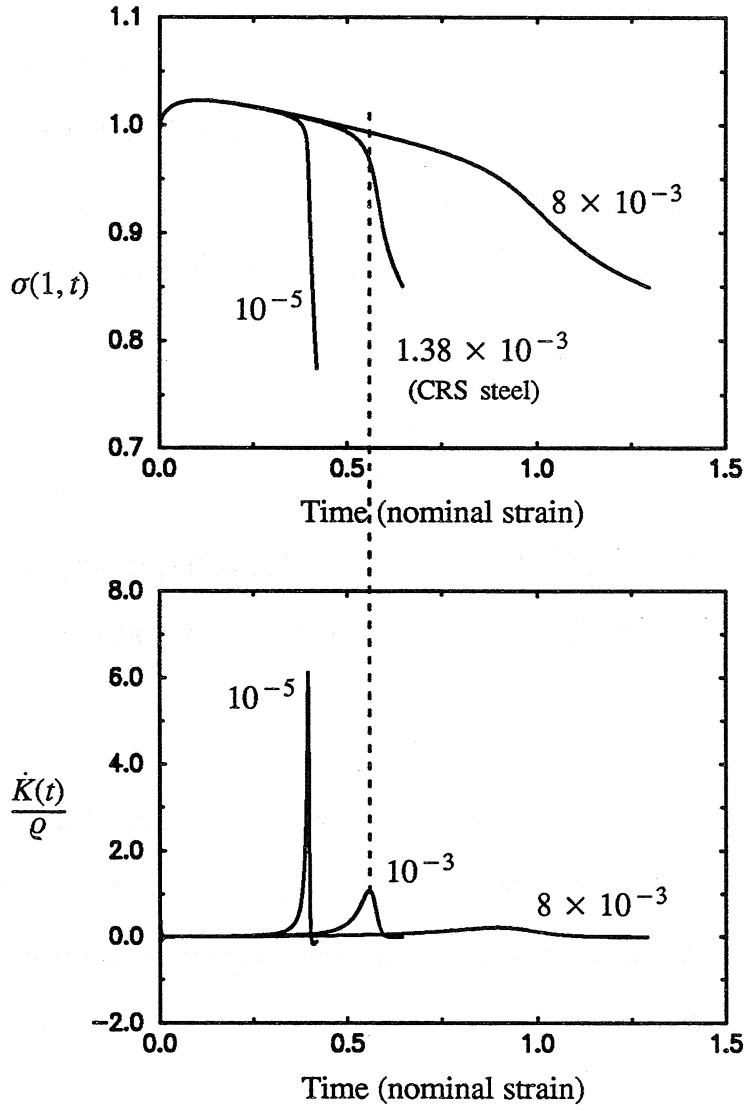

Figure (3) – Effect of the diffusion number on the stress profile at the moving boundary.

As expected, the smaller the diffusion number r_0, the faster is the evolution of localization and the sharper the stress collapse. Comparison of the CRS behavior with that corresponding to

the smaller diffusion number $r_0 = 10^{-5}$ indicates that the assumption of an adiabatic deformation results extremely conservative predictions of the critical localization strains (an error that can be as high as a 100%!).

In Figure (4) , the evolution of displacement profiles is shown for various values of r_0. In all of the considered cases, the maximum time corresponds approximately to the time t_{stb} at which the strain rate attains a maximum. Clearly, smaller diffusion numbers correspond to larger displacement gradients. Once severe localization occurs, the rigid motion of material surrounding the band is quite evident.

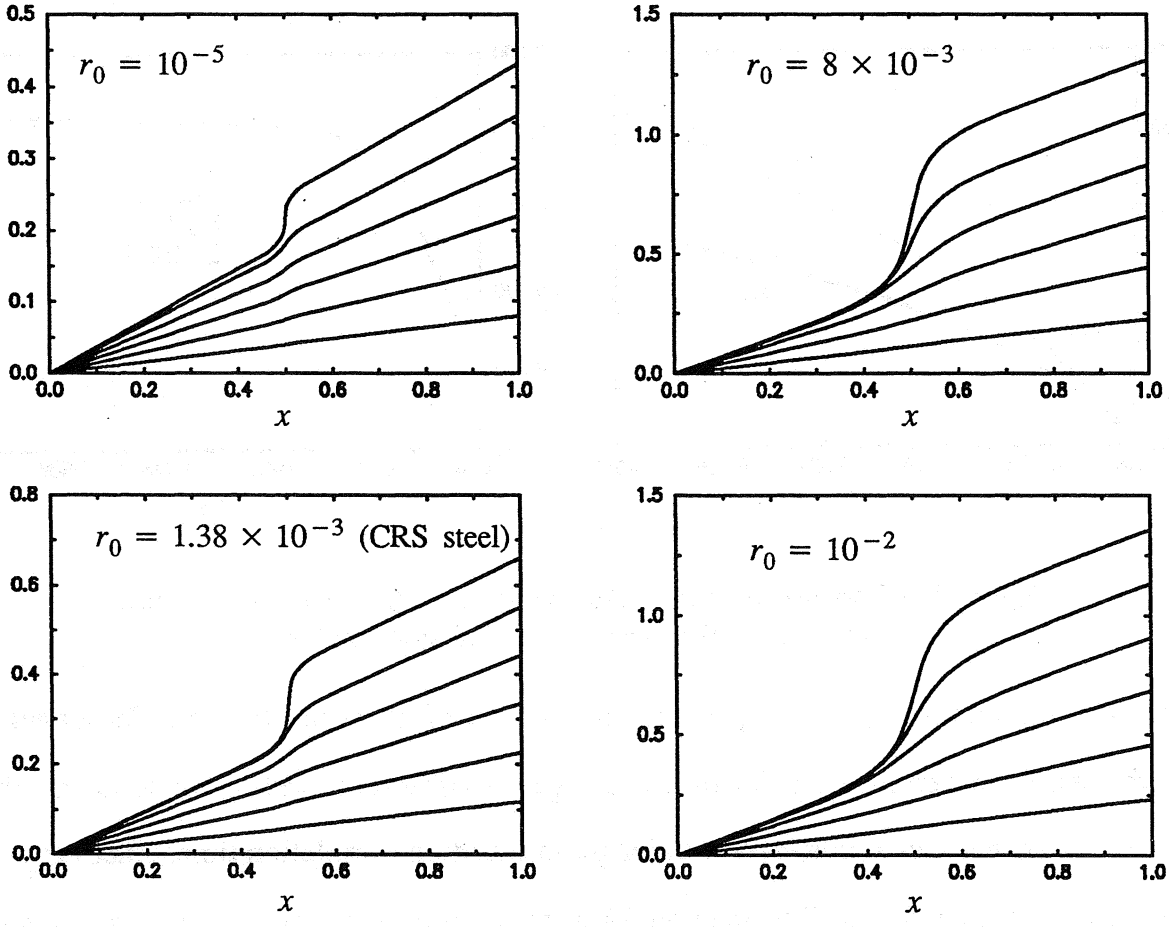

Figure (4) – Displacement profiles for different values of the diffusion number.

Figure (5) illustrates the dependence of various field quantities on the diffusion number[1]. In Figure (5) –(a), the critical times t_{cr} and t_{stb} are plotted against the diffusion number.

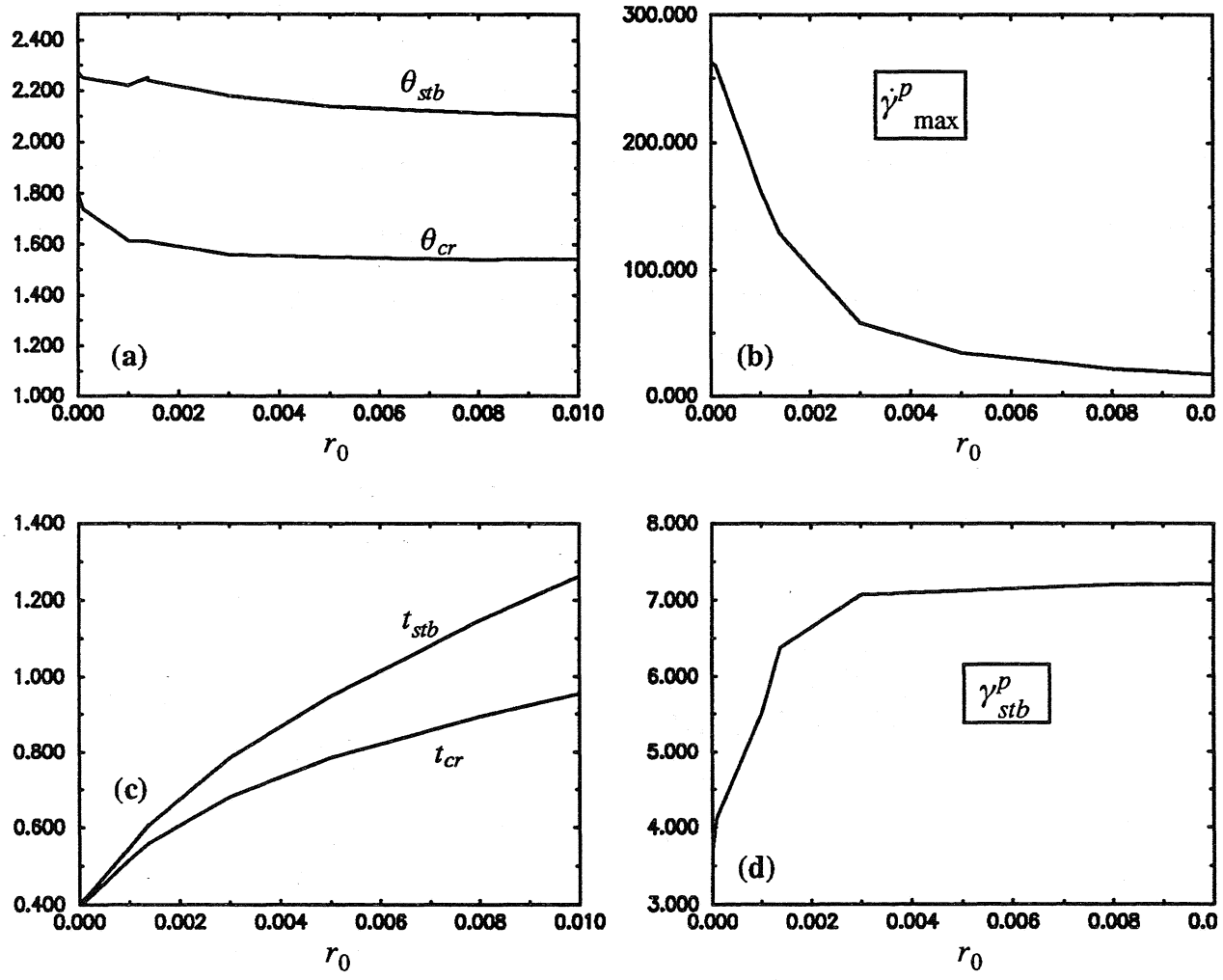

Figure (5) – Variation of various field variables at the center of the band and the critical times with the diffusion number

The difference between t_{cr} and t_{stb} provides the duration of severe localization. The longer the time that it takes to "completely" localize, the larger that difference will be. Thus larger values of the diffusion number r_0 correspond to longer localization completion times since large diffusion numbers allow the locally–generated heat to be conducted away from the band at faster

1. The smallest tested value of the diffusion number is 10^{-5}. Smaller values of the diffusion number result in great numerical difficulties and the loss of band resolution.

rates, thus reducing the severity of localization. Furthermore, for small diffusion numbers (near adiabatic deformations), there is virtually no distinction between the critical times t_{cr} and t_{stb}.

It is interesting to observe that the diffusion number r_0 falls in this region for Kolsky bar tests of most structural steels. Figure (5) −(b) indicates that the temperatures θ_{cr} and θ_{stb} decrease with increasing diffusion numbers while θ_s exhibits a weak dependence on the diffusion number. Moreover, for small diffusion numbers, even though the difference between t_{cr} and t_{stb} is very small, the corresponding differences in temperatures θ_{cr} and θ_{stb} are quite substantial, which is qualitatively consistent with reported experimental findings. Figure (5) −(c) and (d) illustrate the dependence of the maximum strain rate (given by equation (27)) and the central plastic strain, respectively, on the diffusion number. As expected through the examination of expression (27), the maximum strain rate decreases while the central plastic strain increases for increasing values of the diffusion number.

4. The Inertia Number and Localization

This section examines the effect of the inertia number ϱ_0, given by equation (7), on localization while keeping both the diffusion and dissipation numbers fixed. We note that larger values of the applied strain rate or the gauge length render larger inertia numbers. Typical values of the inertia number, for Kolsky bar type experiments, are of the order of 10^{-3}. For this class of deformations, we will show that inertial effects may be ignored which is consistent with observations made by Wright and Walter (1987). However, for applications such as plate–impact tests or the high end of Kolsky bar tests, the quasi–static assumption cannot be made.

4.1. Linear perturbation analysis and inertia number

The linear stability theory provides useful tools towards the derivation of necessary conditions for the *onset* of localization. Mathematical difficulties associated with the implementation of such tools often lead to the assumption of quasi–static deformations for which analytical results may be obtained. The quasi–static assumption is argued to be reasonable as far as the onset of localization is concerned (see Shawki (1993b)). As a result, criteria for the onset of localization obtained through linear perturbation analyses do not provide information regarding the effects of the inertia number ϱ_0.

4.2. Numerical results and discussion

A number of numerical experiments have been carried out by varying the inertia number ϱ_0 while keeping r_0 and r_1 fixed. This is achieved by varying ϕ_0 and H appropriately. The data used is that of a CRS steel (see further details in Cherukuri and Shawki (1993)) except for the value of ϱ_0.

Figure (6) shows the evolution of the stress at the moving boundary (x=1) for various values of the inertia number along with the underlying behavior of the normalized kinetic energy rate. It is evident that rapid stress drop is associated with an extremum value attained by $\dot{K}(t)$.

Furthermore, we note that sharper stress drops are observed for larger inertia numbers. Moreover, profiles associated with inertia numbers less than $O(10^{-2})$ seem to be indistinguishable which indicates that the quasi–static assumption may provide satisfactory description of pre–localization.

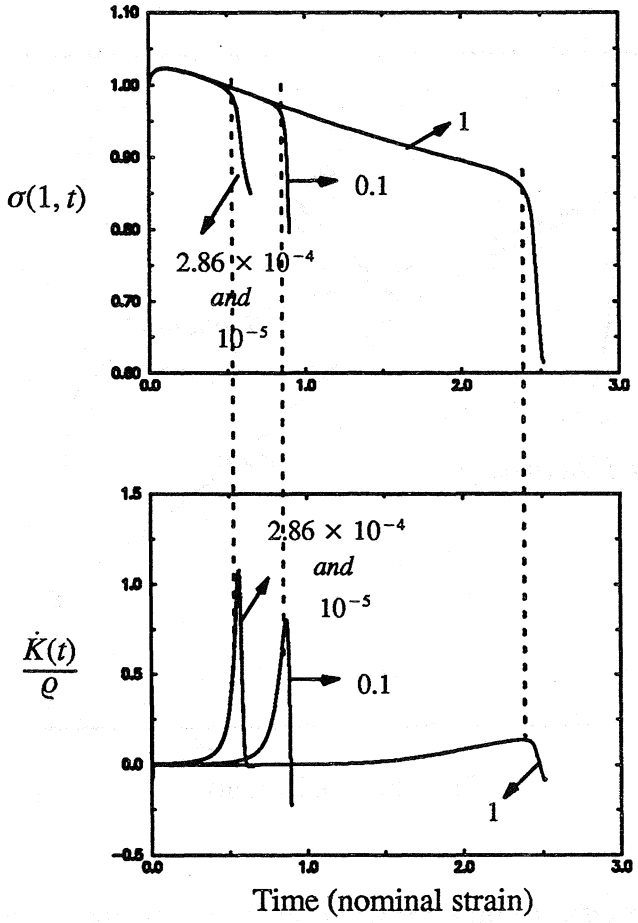

Figure (6) – Evolution of the boundary stress for various values of the inertia number.

To further illustrate this issue, we present the evolution of the band stress as well as the far field stress for two different values of the inertia number as shown in Figure (7) . For the large inertia number, $\varrho_0 = 1$, initial stress evolution is nearly homogeneous while strong stress inhomogeneity develops as soon as localization begins to take place. Further, the band stress drops at a slower rate as opposed to the boundary stress. For the small inertia number, $\varrho_0 = 10^{-5}$, the

two curves are nearly identical implying a near homogeneous stress distribution. In such case, the quasi−static assumption is expected to provide a satisfactory description of localization history. It is also clear that higher values of the inertia number delay the onset of severe localization.

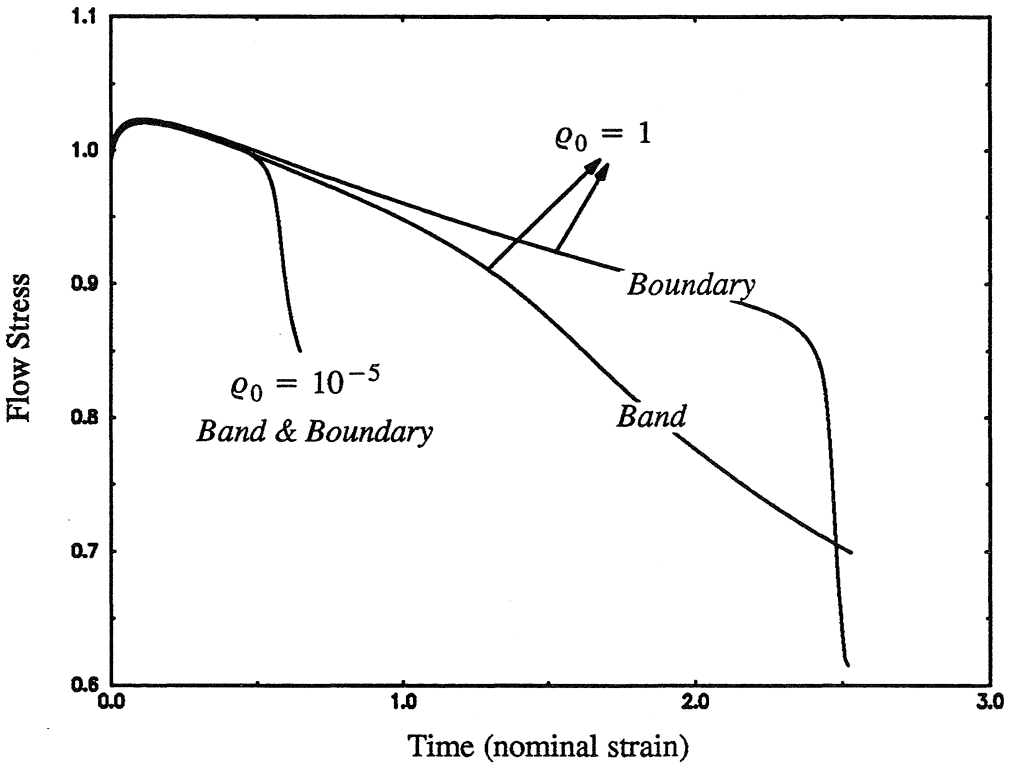

Figure (7) – Stress profile at the band center (x=0.5) and the moving boundary (x=1) for two different values of the inertia number.

The evolution of various field variables is shown in Figure (8) (Figure (9)) for small (large) value of the inertia number ϱ_0. Comparison of the velocity profiles for the two cases indicates that, for large inertia numbers, three distinct spatial regions may be distinguished: (1) a central region where severe localization takes place, (2) a neighboring region in which the deformation becomes progressively more rigid and (3) an outer region where the deformation is nearly homogeneous.

The second region expands into the third region as the deformation continues until it completely absorbs it. For small inertia numbers, on the other hand, the inhomogeneous deformation is seen to take place simultaneously throughout the deforming body. This is also clear from the strain rate plots in the two figures. In the case of small ϱ_0, the strain rate increases in the perturbed region, while simultaneously decreasing outside this region. On the other hand, for large ϱ_0, there seems to be a wave–like behavior through which region 2 expands into region 3. Further, the larger the inertia number, the smaller is the maximum strain rate and consequently the wider is the shear band.

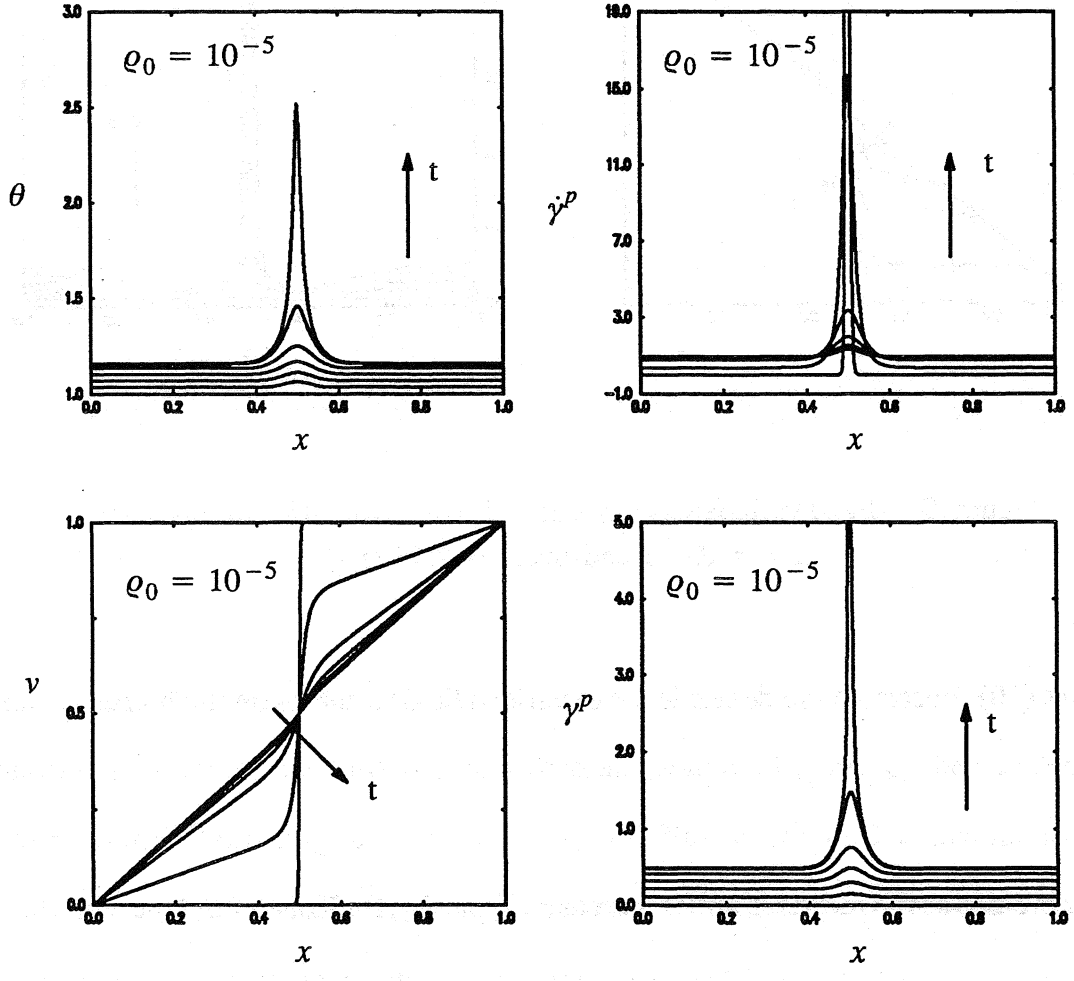

Figure (8) – Field variables as functions of position at different times
$\Delta t = 0.101$ and $\max t = 0.606$ (t_{stb})

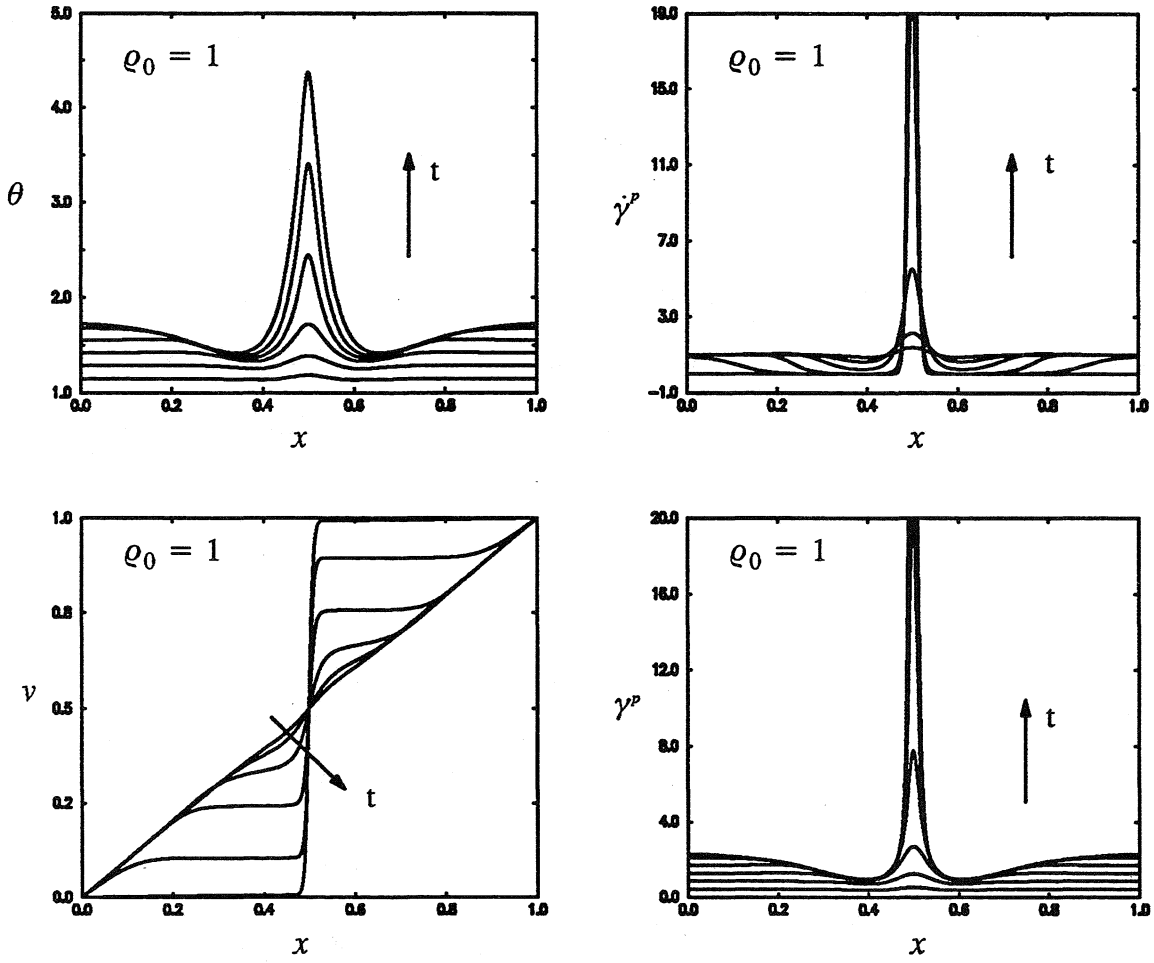

Figure (9) – Field variables as functions of position at different times with $\Delta t = 0.425$ and $\max t = 2.55$ (t_{stb})

Figure (10) illustrates the dependence of various field variables on the inertia number ϱ_0 at the times t_{cr} and t_{stb}. As ϱ_0 increases, the critical time t_{cr} (or the critical nominal strain) for localization increases. Initially, the difference between t_{cr} and t_{stb} is small. However, this difference increases as the inertia number increases. Typically, for Kolsky bar type tests, the inertia number is of the order of 10^{-4} and hence for these tests, localization, once it begins, proceeds very quickly. The maximum strain rate at the center of the band decreases with increasing ϱ_0. Our numerical results indicate that for very small values of ϱ_0 the maximum

strain rate remains approximately constant indicating again that the quasi–static assumption is a valid approximation for Kolsky bar type experiments.

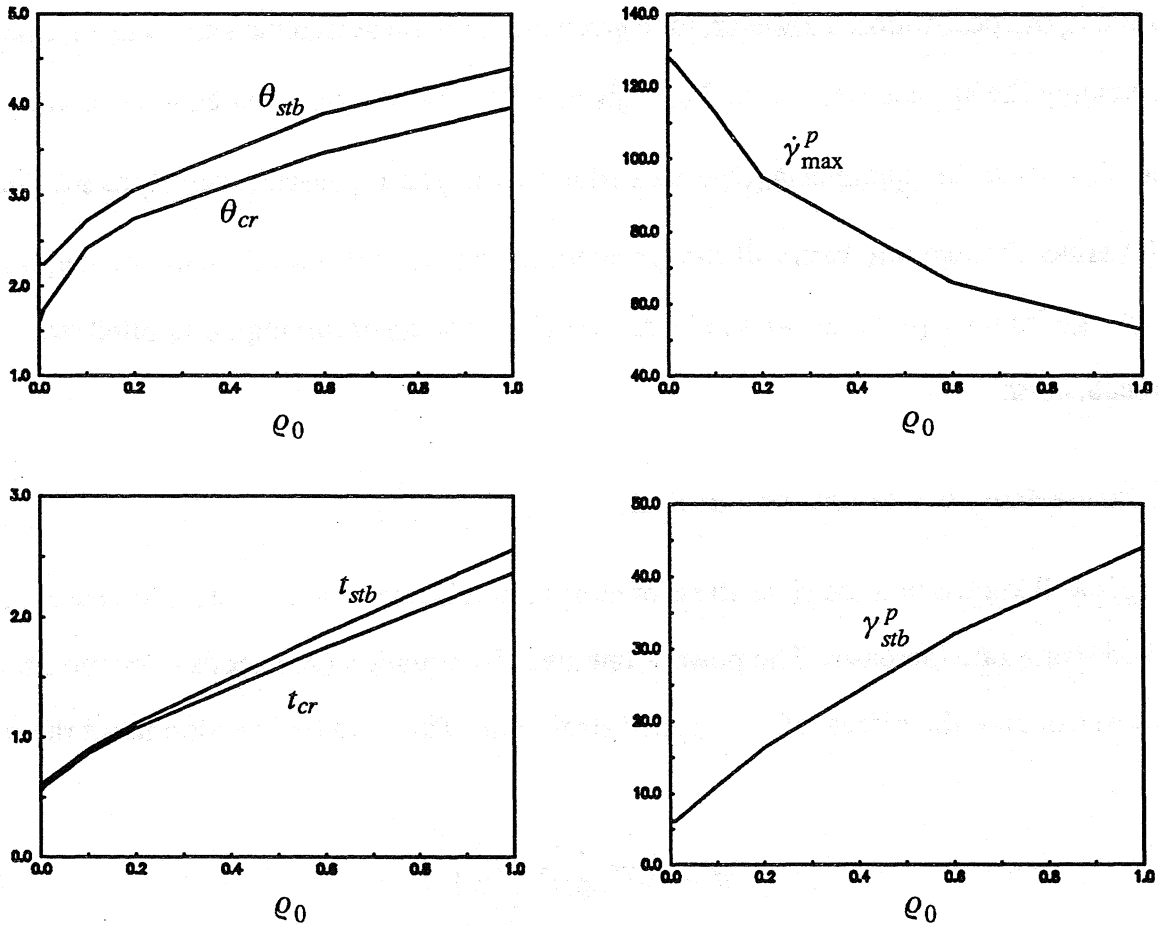

Figure (10) – Variation of various variables with the inertia number.

4.3. Shear band width and the inertia number

Figure (10) indicates that the maximum strain rate at the center (at time t_{stb}), decreases with increasing the inertia number. Since the total strain rate is constant and since the elastic strain rate is much smaller than the plastic strain rate, this implies that the shear band width increases with increasing the inertia number. Our results indicate that in the limit of a vanishing inertia number, the band width remains finite in the presence of heat conduction.

5. Applied Strain Rate and Localization

In previous sections, we examined the effects of the inertia number ϱ_0 and the diffusion number r_0 on localization. However, for a given material, these numbers can only be changed by changing the applied strain rate. For a given material and a given specimen geometry, ϱ_0 varies directly as the square of $\hat{\phi}_0$ (the applied strain rate) and r_0 varies inversely as $\hat{\phi}_0$. Thus, if $\hat{\phi}_0$ is varied, the two numbers will change simultaneously. In this section, drawing upon our knowledge from the previous two sections, we study the effect of varying the applied strain rate on localization.

5.1. Numerical results and Discussion

It is well known that the yield stress of most metals is rate sensitive i.e., it increases as the applied strain rate increases. The power−law given by equation (21) needs to be modified in order to examine the effects of the applied strain rate. The modified version takes the form

$$\sigma = (\theta)^{\nu} \left(\frac{\gamma}{\gamma_0}\right)^{n} \left(\frac{\dot{\gamma}^p}{\dot{\gamma}^p_n}\right)^{m}, \tag{30}$$

where $\dot{\gamma}^p_n$ is the non−dimensional strain rate used as a reference strain rate in obtaining the power law. It is to be noted that the corresponding dimensional strain rate $\hat{\dot{\gamma}}^p_n$ is different in general from the applied strain rate $\hat{\phi}_0$ which apart from being the applied strain rate is also used to non−dimensionalize the governing equations. Here, we take $\hat{\dot{\gamma}}^p_n$ to be equal to 1600/s. At this point, we emphasize that the power−law is an empirical formula which provides a satisfactory description of material response over a specific range of applied strain rates (typically the range of strain rates associated with the Kolsky bar test). Therefore; extrapolation of the results to higher strain rates must be conducted with caution.

Several numerical experiments have been carried out by changing the applied strain rate. The data corresponds to the CRS steel. The evolution of the kinetic energy rate $\dot{K}(t)$ and the boundary stress $\sigma(1,t)$ are shown in Figure (11) .

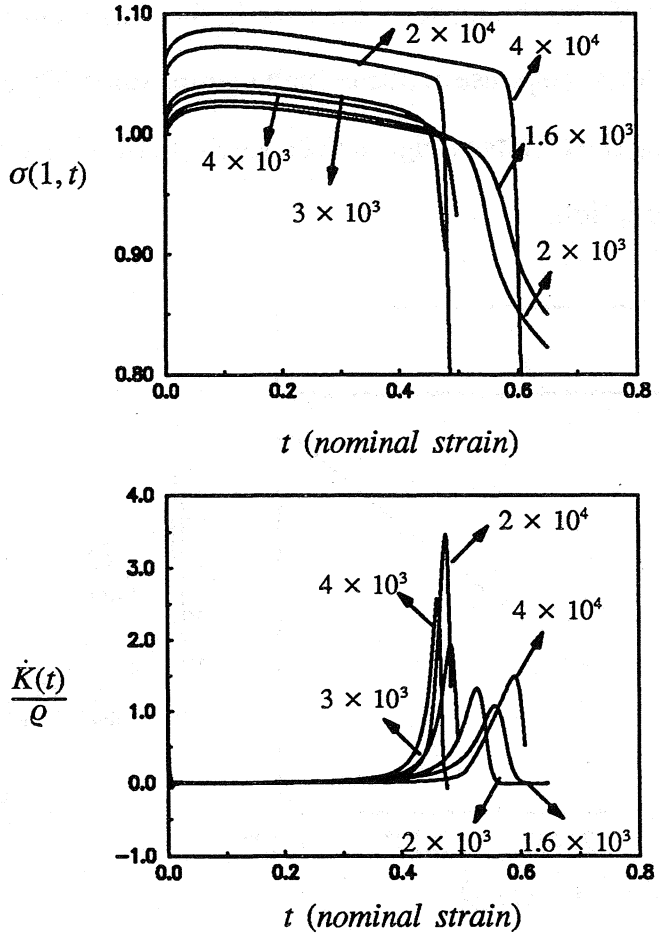

Figure (11) – Evolution of the boundary stress for different applied strain rates.

Clearly, larger values of the applied strain rate correspond to larger yield stresses. As $\hat{\phi}_0$ increases, the critical time for the onset of localization t_{cr} decreases. Then once a critical strain rate is exceeded, the critical localization time t_{cr} starts increasing as shown in Figure (12) . Hence, there exists a critical strain rate at which the localization occurs the fastest. The falling branch in Figure (12) has a larger slope than that of the rising branch.

Further examination of Figure (11) indicates that, when localization takes place, the drop in stress is much sharper for higher strain rates than it is for lower strain rates. It is also useful to note that the initial yield stress is weakly sensitive to the applied strain rate since a 20−fold increase in the applied strain rate leads to an increase in the initial yield stress by only 10 percent. This behavior is specific to the power−law constitutive form and may not adequately describe the observed material response at ultra−high loading rates. Therefore; caution must be exercised in interpreting the results of Figure (12) which are obtained by using the power−law form of material description.

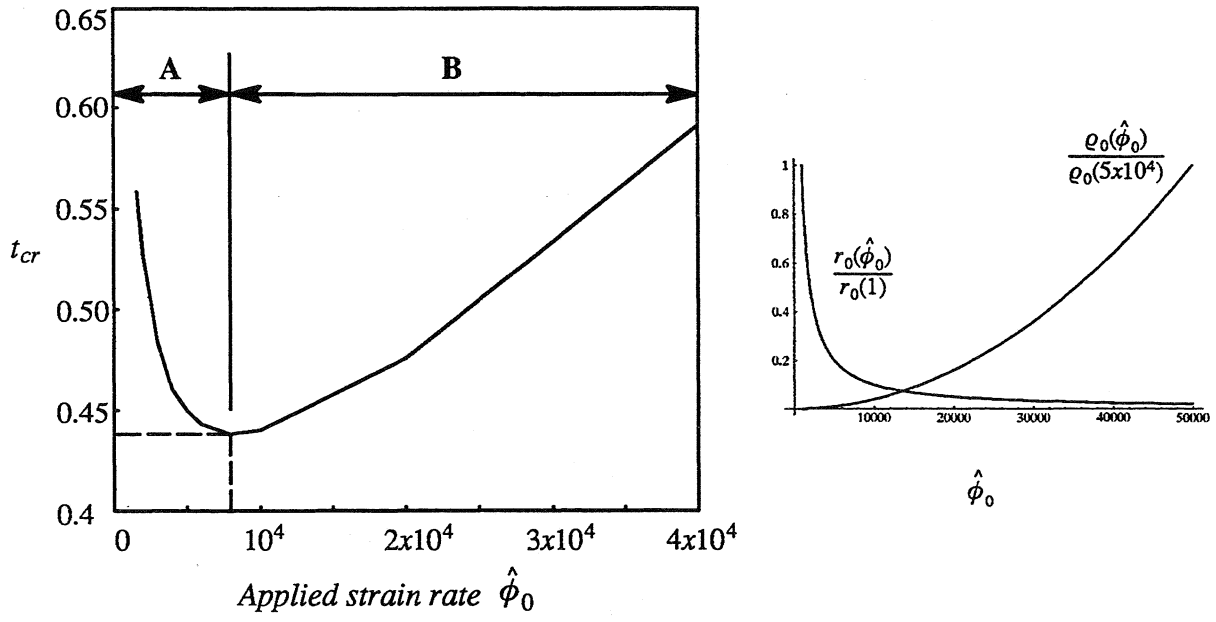

Figure (12) – Critical localization time as a function of the applied strain rate.

In an attempt to rationalize the behavior shown in Figure (12) , we note that the critical localization time t_{cr} increases with increasing values of the inertia and diffusion numbers. Moreover, the inertia number is proportional to the square of the applied strain rate while the diffusion number is inversely proportional to the applied strain rate; i.e.

$$\varrho_0 \sim \hat{\phi}_0^{\,2} \quad \text{and} \quad r_0 \sim 1/\phi_0 \tag{31}$$

The insert in Figure (12) illustrates the dependence of the normalized inertia and diffusion numbers on the applied strain rate for the considered material and geometry. It is evident that, in regime A, the fast decay in the diffusion number tends to accelerate localization beyond the stabilization effect introduced through the increase of the inertia number. In regime B, the faster increase in the inertia number offsets the effect of diffusion number decay and, therefore, results in the observed increase in the critical localization time.

5.2. Shear band width and the applied strain rate

Our numerical results show that the maximum plastic strain rate $\dot{\gamma}_{\max} \equiv \dot{\gamma}^p(0.5, t_{stb})$ increases with increasing the applied strain rate. For example, $\dot{\gamma}_{\max}$ is equal to approximately 128 when $\hat{\dot{\phi}}_0$= 1600/s and is equal to approximately 550 when $\hat{\dot{\phi}}_0$= 10000/s. Thus, as the applied strain rate increases, the band width decreases. This is indicative of the role that the diffusion number r_0 plays in determining the band width. Furthermore, it is important to note that the reduction in band thickness due to the decay in the diffusion number overwhelms the increase in band thickness due to increasing values of the inertia number.

Since the band width is inversely proportional to the applied strain rate, sufficiently refined meshes are used to obtain the numerical results for high applied strain rates (e.g. for an applied strain rate of 10000/s, the total number of grid divisions used is 1000).

6. Dissipation Number and Localization

This section examines the effect of the dissipation number $r_1 = \beta\hat{\sigma}_0/\hat{\varrho}\hat{c}\hat{\theta}_0$ on localization. For Kolsky bar experiments of structural steels at room temperature, the dissipation number has a value of approximately 0.25. On the other hand, for a Tungsten Heavy Alloy, it assumes a value of approximately 1.3. Larger values of the dissipation number lead to the generation of more thermal energy per unit time which tends to accelerate localization. Thus, if the inertia and diffusion numbers are small, localization is expected to take place faster in Tungsten Heavy Alloys than in steels. Guided by earlier observations, it appears that localization is weakly sensitive to both the inertia and diffusion numbers in their low−end values (i.e. if they are sufficiently small). The present study illustrates that localization is strongly sensitive to variations of the dissipation number.

6.1. Localization criteria from linear perturbation analysis

For a strain−independent, thermally−sensitive power law type material, the necessary condition for localization is given by the inequality (18) which reduces to (19) in the absence of heat conduction effects. The condition (19) implies that for adiabatic deformations, the necessary condition for localization is insensitive to the dissipation number r_1. This observation illustrates that the *onset* of localization may be insensitive to localization while it does not provide information as to the effect of dissipation on post−localization. However, in the presence of heat conduction, as (18) indicates, the effect of r_1 is to counteract the stabilizing behavior of heat conduction. It will be shown in this section that this is consistent with the fully non−linear results.

6.2. Numerical Results and Discussion

Several numerical experiments have been carried out to study the effect of dissipation number on localization. The inertia number and the diffusion number are kept fixed at the values for the case studied in section 4 for CRS steel.

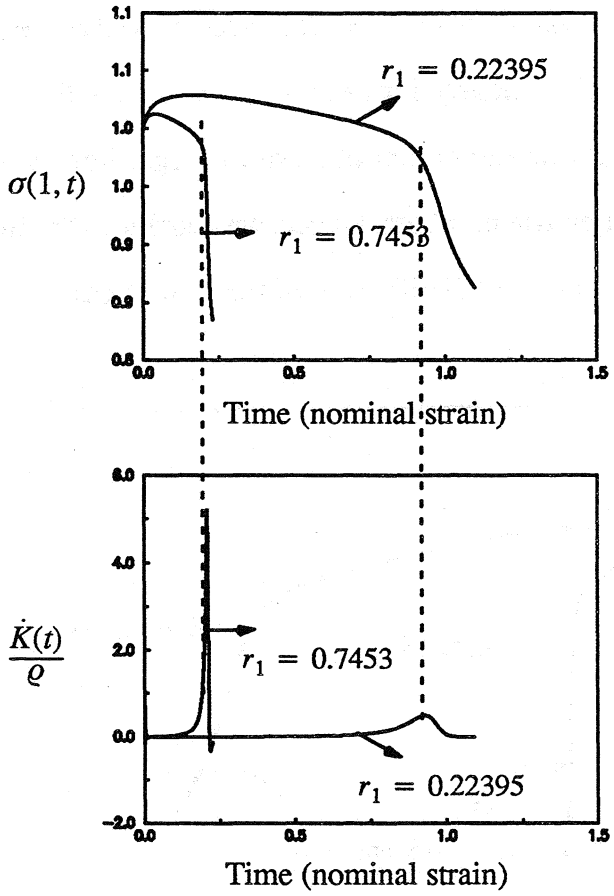

Figure (13) – Evolution of the boundary stress for various values of the dissipation number.

Figure (13) illustrates the evolution of the stress at the moving boundary along with the evolution of the normalized kinetic energy rate for two different values of the dissipation number. It is evident that localization develops at a faster rate for the case corresponding to the larger dissipation number. Furthermore, for larger values of r_1, thermal softening overwhelms hardening mechanisms at smaller values of the nominal strains leading to a shorter hardening branch of the stress–strain curve. Moreover, the flow stress exhibits a sharper drop during localization for larger values of the dissipation number. Another interesting observation relates to the smaller critical localization times (for larger dissipation numbers) being associated with larger values of $\dot{K}(t_{cr})$.

Figure (14) shows the evolution of the boundary stress as well as the band stress for the two cases presented in Figure (13) . Clearly, for each of the two cases, the two stresses are almost identical which is consistent with our earlier observation regarding the validity of the quasi–static assumption for small inertia numbers. Hence, we conclude that the dissipation number has a negligible effect on the spatial distribution of the flow stress.

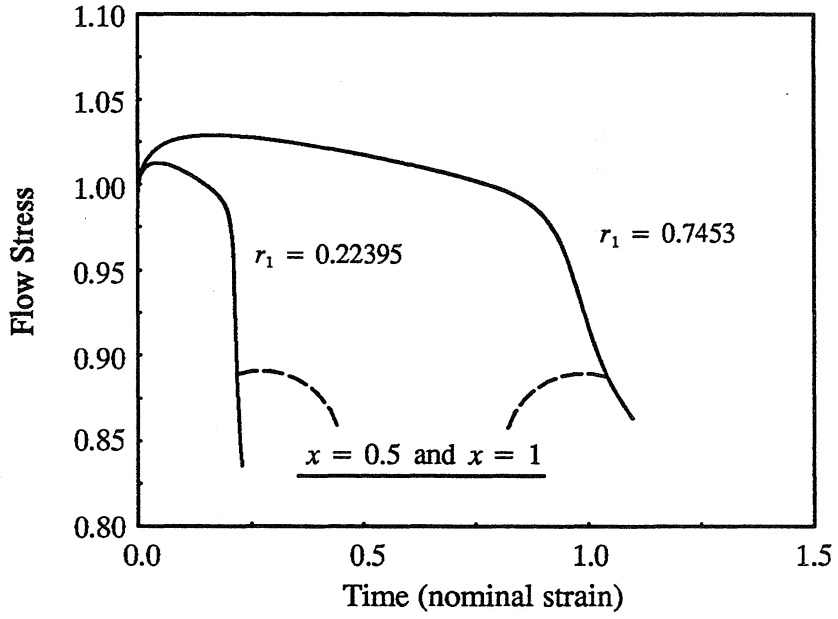

Figure (14) – Evolution of the band and boundary stresses for two different values of the dissipation number

Figure (15) provides the displacement profiles for the two considered. Each computation is carried out up to its associated stabilization time t_{stb}. Here, we note that as r_1 increases, the nominal strain and hence the maximum displacement at $x = 1$ decreases. Furthermore, it is evident that the band width increases with decreasing values of the dissipation number. This numerical observation is consistent with the linear stability prediction (see Shawki (1993a)) in which the critical wave length of perturbations is given by

$$l_{cr} = \sqrt{\frac{r_o}{r_1(p-1)}} \ . \tag{32}$$

for a power–law material with $n = 0$ and $p = -\nu/m > 1$. Shawki (1993a) showed that the foregoing wavelength threshold represents the minimum below which initial perturbations do not grow due to the early stabilizing effect of heat conduction. Moreover, Sherif and Shawki (1992) showed through a late–time steady–state solution that the minimum shear band width is proportional to $\sqrt{r_0/r_1}$. Hence, results obtained through the linear stability analysis (Shawki (1993b)), late–time analytic steady–state (Sherif and Shawki (1992)), and the present numerical solutions confirm the aforementioned functional dependence of shear band thickness.

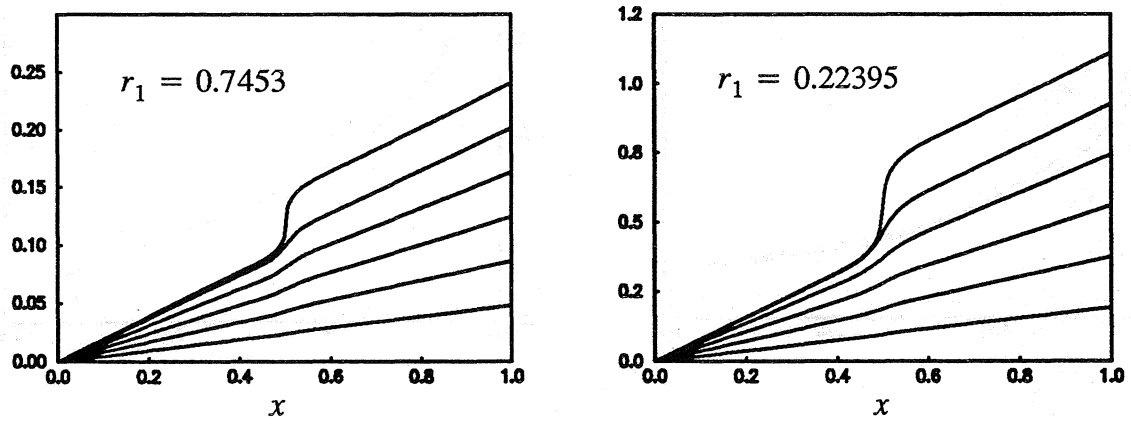

Figure (15) – Displacement profiles for two different values of the dissipation number

Figure (16) shows the variation of various field variables with respect to r_1 at the times t_{cr}, and t_{stb}. As r_1 increases, the critical time t_{cr} for localization (equivalently, the critical nominal strain) decreases in a near–exponential fashion. Furthermore, the difference between t_{cr} and t_{stb} decreases as r_1 increases. Hence, localization takes place at a much faster rate for large values of the dissipation number. Further examination of Figure (16) indicates that the critical temperature $\theta_{cr} \equiv \theta(0.5, t_{cr})$ is weakly proportional to r_1 while the maximum strain rate increases with r_1. On the other hand, the critical strain $\gamma_{cr} \equiv \gamma(0.5, t_{cr})$ is inversely proportional to r_1.

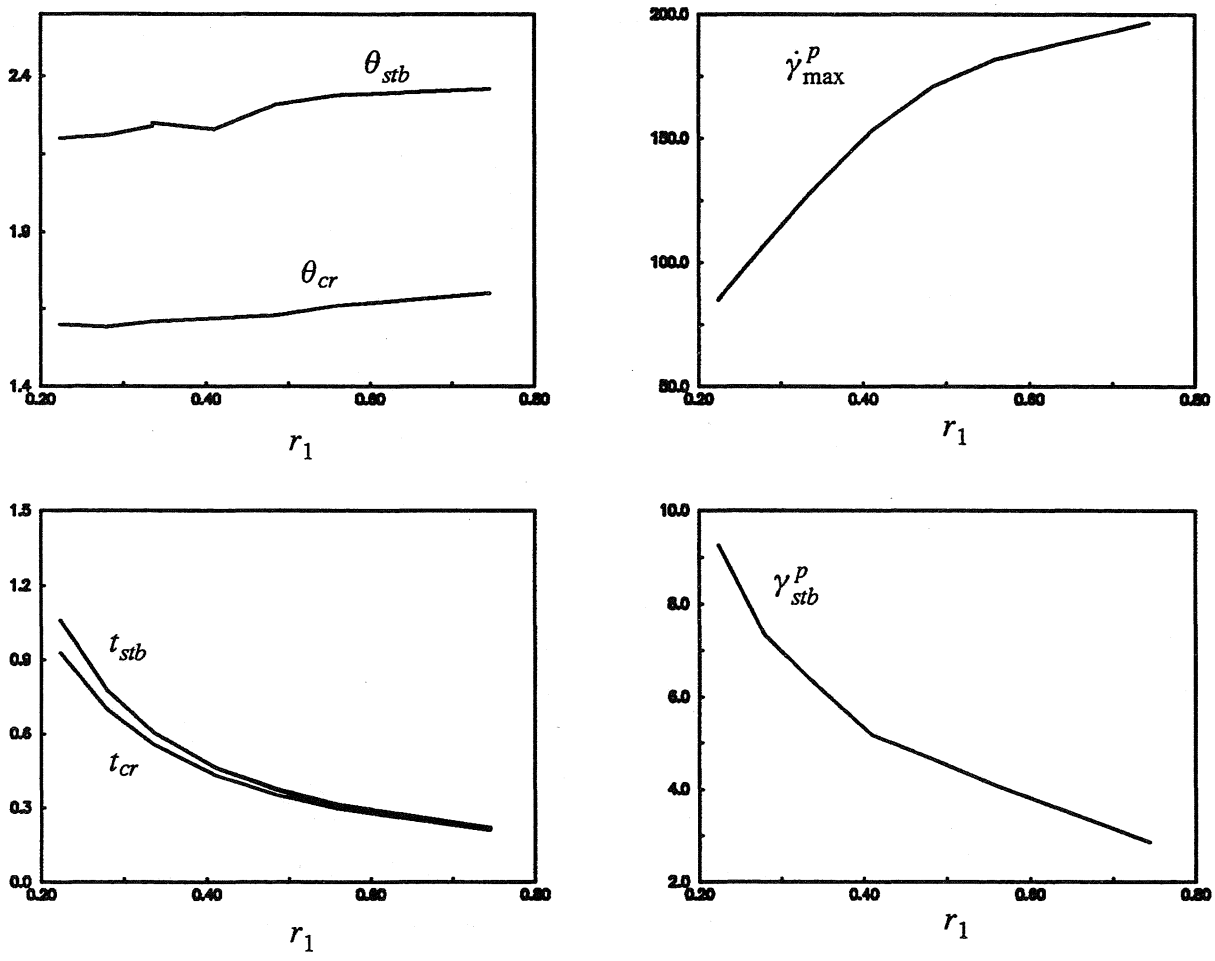

Figure (16) – Variation of various field variables with the dissipation number

7. Discussion

We take advantage of the results of previous sections towards the determination of the *localization sensitivity* of various engineering materials. Therefore, we consider a number of materials that have been reported to localize under favorable experimental conditions.

7.1. Some experimental results and non–dimensional numbers

The following table summarizes the thermo–mechanical properties of the considered materials:

Table 2 – Thermo–mechanical properties of selected engineering materials.

Material	Density (kg/m^3)	Specific Heat (J/kg–K)	Thermal conductivity (W/m–K)	Shear Modulus (GPa)	Initial Yield Stress (GPa)
CRS steel	7800	500	54	81	436
HRS steel	7800	500	54	81	261
HY–100	7800	500	54	81	530
4340 (HRC 44)	7800	500	54	81	800 (approx)
4340 (HRC 55)	7800	500	54	81	1020 (approx)
Copper	8960	385	400		200*
WHA	17140	139	75	134	900

* extrapolated from the data given in[8].

The critical nominal strains for localization for these materials at an applied strain rate of approximately (1000/sec) are presented in Table 3. For the times that the Kolsky bar tests were conducted on copper specimens, no localization was observed. We note that the HRS steel is the slowest to localize, the 4340 (HRC 55) is the fastest whereas the CRS steel and the HY–100 localize at about the same nominal strain.

Table 3 – Critical localization strains for selected engineering materials.

Material	Critial Strain
CRS steel	0.5
HRS steel	1.0(approx)
HY–100	0.45
4340 (HRC 44)	0.2
4340 (HRC 55)	0.15
copper	no band observed*
WHA	0.15 (approx)

*For the times that the tests were made, no band has been observed[4]

Table 4 summarizes the dimensionless values of the inertia number ϱ_0, the diffusion number r_0 and the dissipation number r_1 for the considered materials at an applied strain rate of 1000/sec. The gauge length is taken to be 0.0025m for all the materials.

Table 4 – Typical values of the dimensionless numbers for selected engineering materials.

material \ Number	inertia number	diffusion number	dissipation number
CRS steel	0.0001118	0.0022154	0.3354
HRS steel	0.0001868	0.0022154	0.2008
HY–100	0.0000920	0.0022154	0.4077
4340 (HRC 44)	0.0000609	0.0022154	0.6154
4340 (HRC 55)	0.0000478	0.0022154	0.7846
WHA	0.0001190	0.0050368	1.1333
Copper	0.0002800	0.0185530	0.1740

Upon comparing Tables 3 and 4, we observe that the larger the dissiaption number, the smaller the critical nominal strain at which localization occurs which is consistent with our foregoing numerical results. Furthermore, we note that the diffusion number is the same for all the steels while they have different values of ϱ_0 and r_1. For structural steels deforming at strain rates lower than 10^4 per sec, the effect of ϱ_0 can be practically ignored. Thus, for structural steels, the most significant dimensionless number that influences localization sensitivity appears to

be the *dissipation number*. Examination of Table 3 confirms that the HRC 55 is the steel with the largest dissipation number, in the considered material selection for steels, which localizes at the smallest nominal strain. Moreover, experimental results indicate that the shear band width is the smallest for this steel. This is consistent with our discussion in section 6. where we noted that the larger the dissipation number, the larger is the maximum strain rate at the center of the band and consequently the thinner is the band. The tungsten heavy alloy (WHA) has the largest dissipation number in Table 4. However, its diffusion number is about twice that of the considered steels. Consequently, due to the stabilizing effects of heat conduction, the WHA localizes at nearly the same nominal strain as the 4340 (HRC 55) steel. Examination of the dimensionless numbers for Copper, we note that the inertia number is about 5 times that of HRS steel while the diffusion number is about 9 times larger than that of steels. The dissipation number is also smaller than that of HRS steel. Hence, Copper is expected to localize at relatively large nominal strains (if any).

Acknowledgments

The support of the National Science Foundation to (TGS) through the Presidential Young Investigator Award # NSF MSS 89−57180 PYI is gratefully acknowledged. Computer donations from the Hewlett Packard Company and the NeXT Computer Company to the University of Illinois have made the computations possible. These donations are appreciated. The authors would like to acknowledge the fruitful discussions with Professor Rodney Clifton, Professor Jack Duffy and E. Andrews.

References

1. Dodd, B. and Bai (1985), Y. L., Adiabatic shear band width, *Mat. Sci. Tech.*, Vol. 1, pp. 38−40.

2. Gioia, G. and Ortiz, M. (1992), work in progress.

3. Marchand, A. and Duffy, J. (1988), An experimental study of the formation process of adiabatic shear bands in a structural steel, *J. Mech. Phys. Solids*, Vol. 36, No. 3, pp. 251−283.

4. Merzer, A. M. (1982), Modelling of adiabatic shear band development from small imperfections, *J. Mech. Phys. Solids*, Vol. 30, No. 5, pp. 323−338.

5. Shawki, T. G. (1988), Necessary and Sufficient Conditions for localization in thermal viscoplastic materials, TAM report No. 489, UIUC.

6. Shawki, T.G. (1992), The Phenomenon of Shear Strain Localization in Dynamic Viscoplasticity, *Appl. Mech. Rev.*, Vol. 45, No. 3, Part 2, pp. 46−61

7. Shawki, T. G., Sherif, R. A. and Cherukuri, H. P. (1992), Characterization of the flow localization history in dynamic viscoplasticity, *Appl. Mech. Rev.*, Vol. 45, No. 3, part 2, pp. 149−153.

8. Shawki, T.G. (1993a), An Energy Criterion for the Onset of Shear Localization in Thermal Viscoplastic Materials−Part I: Necessary and Sufficient Initiation Conditions, *J. Appl. Mech.*, to appear.

9. Shawki, T.G. (1993b), An Energy Criterion for the Onset of Shear Localization in Thermal Viscoplastic Materials−Part II: Applications and Implications, *J. Appl. Mech.*, to appear.

10. Shawki, T. G. and Clifton, R. J. (1989), Shear band formation in thermal viscoplastic materials, *Mech. of Materials*, Vol. 8, No. 1, pp. 13−43.

11. Sherif, R. A. and Shawki, T. G. (1992), The role of heat conduction during the post−localization regime in dynamic viscoplasticity, AMD−Vol. 135, ASME publication, Plastic Flow and Creep, Ed. by Zbib H. M., pp. 159−173.

12. Wright, T. W. and Walter J. W. (1987), On stress collapse in adiabatic shear bands, *J. Mech. Phys. Solids*, Vol. 35, No. 6, pp. 701−720.

13. Wright, T. W. (1992), A model for the fully formed shear bands, *J. Mech. Phys. Solids*, Vol. 40, No. 6, pp. 1217−1226.

14. Zbib HM and Jubran JS (1992), Dynamic shear banding: A three−dimensional analysis, to appear in the *Int J Plasticity*.

List of Recent TAM Reports

No.	Authors	Title	Date
494	Toro, J. R.	Existence of weak solutions to the thick plate problem with various boundary conditions	Apr. 1989
495	Stewart, D. S., and B. W. Asay	Discrete modeling of beds of propellant exposed to strong stimulus	Apr. 1991
496	Klein, R., and D. S. Stewart	The relation between curvature, rate state dependence, and detonation velocity	Apr. 1991
497	Powers, J. M., and D. S. Stewart	Approximate solutions for oblique detonations in the hypersonic limit	Apr. 1991
498	Davidson, M. T., K. L. Kuster, K. W. Quinn, N. A. Sluz, and G. Stojkovich	Twenty-fifth student symposium on engineering mechanics, M. E. Clark, coord. (1988)	Feb. 1992
499	Cardenas, H. E., W. C. Crone, D. J. Scott, G. G. Stewart, and B. F. Tatting	Twenty-sixth student symposium on engineering mechanics, M. E. Clark, coord. (1989)	Mar. 1992
700	Juister, C. E., D. W. Newport, C. S. Payne, J. M. Peters, M. P. Thomas, and J. C. Trovillion	Twenty-seventh student symposium on engineering mechanics, M. E. Clark, coord. (1990)	Apr. 1992
701	Bernard, R. T., D. W. Claxon, J. A. Jones, V. R. Nitzsche, and M. T. Stadtherr	Twenty-eighth student symposium on engineering mechanics, M. E. Clark, coord. (1991)	Apr. 1992
702	Greening, L. E., P. J. Joyce, S. G. Martensen, M. D. Morley, J. M. Ockers, M. D. Taylor, and P. J. Walsh	Twenty-ninth student symposium on engineering mechanics, J. W. Phillips, coord. (1992)	May 1992
703	Kuah, H. T., and D. N. Riahi	Instabilities and transition to chaos in plane wakes	Nov. 1992
704	Stewart, D. S., K. Prasad, and B. W. Asay	Simplified modeling of transition to detonation in porous energetic materials	Nov. 1992
705	Stewart, D. S., and J. B. Bdzil	Asymptotics and multi-scale simulation in a numerical combustion laboratory	Jan. 1993
706	Hsia, K. J., Y.-B. Xin, and L. Lin	Numerical simulation of semi-crystalline Nylon 6: Elastic constants of crystalline and amorphous parts	Jan. 1993
707	Hsia, K. J., and J. Q. Huang	Curvature effects on compressive failure strength of long fiber composite laminates	Jan. 1993
708	Jog, C. S., R. B. Haber, and M. P. Bendsoe	Topology design with optimized, self-adaptive materials	Mar. 1993
709	Barkey, M. E., D. F. Socie, and K. J. Hsia	A yield surface approach to the estimation of notch strains for proportional and nonproportional cyclic loading	Apr. 1993
710	Feldsien, T. M., A. D. Friend, G. S. Gehner, T. D. McCoy, K. V. Remmert, D. L. Riedl, P. L. Scheiberle, and J. W. Wu	Thirtieth student symposium on engineering mechanics, J. W. Phillips, coord. (1993)	Apr. 1993
711	Weaver, R. L.	Anderson localization in the time domain: Numerical studies of waves in two-dimensional disordered media	Apr. 1993
712	Cherukuri, H. P., and T. G. Shawki	An energy-based localization theory: Part I—Basic framework	Apr. 1993
713	Manring, N. D., and R. E. Johnson	Modeling a variable-displacement pump	June 1993
714	Birnbaum, H. K., and P. Sofronis	Hydrogen-enhanced localized plasticity—A mechanism for hydrogen-related fracture	July 1993
715	Balachandar, S., and M. R. Malik	Inviscid instability of streamwise corner flow	July 1993
716	Sofronis, P.	Linearized hydrogen elasticity	July 1993
717	Nitzsche, V. R., and K. J. Hsia	Modelling of dislocation mobility controlled brittle-to-ductile transition	July 1993
718	Hsia, K. J., and A. S. Argon	Experimental study of the mechanisms of brittle-to-ductile transition of cleavage fracture in silicon single crystals	July 1993
719	Cherukuri, H. P., and T. G. Shawki	An energy-based localization theory: Part II—Effects of the diffusion, inertia and dissipation numbers	Aug. 1993